

# Tuning of structural color using a dielectric actuator and multifunctional compliant electrodes

Zhao H. Fang,<sup>1</sup> Christian Punckt,<sup>1</sup> Eva Y. Leung,<sup>1</sup> Hannes C. Schniepp,<sup>1,2</sup>  
and Ilhan A. Aksay<sup>1,\*</sup>

<sup>1</sup>Department of Chemical and Biological Engineering, Princeton University, Princeton, New Jersey 08544, USA

<sup>2</sup>Currently with the Department of Applied Science, The College of William and Mary,  
Williamsburg, Virginia 23187, USA

\*Corresponding author: iaksay@princeton.edu

Received 2 August 2010; revised 4 October 2010; accepted 22 October 2010;  
posted 26 October 2010 (Doc. ID 132659); published 1 December 2010

We have developed electrically conducting silicone elastomer nanocomposites that serve both as compliant electrodes in an electrostatic actuator and, at the same time, as optically active elements creating structural color. We demonstrate the capabilities of our setup by actuating an elastomeric diffraction grating and colloidal-crystal-based photonic structures. © 2010 Optical Society of America  
*OCIS codes:* 160.0160, 000.2170.

## 1. Introduction

Materials exhibiting structural color, i.e., color caused at least in part by elastic interactions of light with matter, are ubiquitous in nature [1–5]. They are nonbleachable and can possess a narrow optical bandwidth. In particular, dynamic structural color materials, i.e., materials in which the variation of an externally controllable parameter causes a dynamic optical response, such as a wavelength shift, have been in the focus of research recently, due to a wide range of applications in the fields of display devices [6–9], chemical and mechanical sensors [6,10–14], and tunable organic lasers [15].

For the active dynamic tuning of the optical properties of such materials, a variety of methods has been proposed, ranging from direct mechanical manipulation of photonic elastomers [12,16,17] to electrochemical actuation and swelling of block copolymers [7,13,18–20], methods based on electrochemical processes in polyelectrolytes [21] or polymers [22,23], infiltration of liquids into the voids between hollow spheres [24], and thermal actuation [6,25–27]. Also, microelectromechanical systems

(MEMS) and piezoelectric devices have been employed [25,27–30]. Especially for use in dynamic display devices, materials should be tunable by an electric signal and possess both a sufficiently large tuning range (e.g., optical band shift) as well as a rapid response time [22]. Actuation based on thermal effects, swelling, or electrochemical processes is intrinsically slow because it is limited by diffusion. MEMS and piezoelectric devices are fast but have only a limited tuning range.

A promising approach for combining rapid response time and large actuation amplitude is the use of dielectric actuators [31–33], also known as “artificial muscles,” which can be driven at acoustic frequencies [34] and exceed strains of 100% [31]. A field-type elastomeric actuator requires mechanically compliant electrodes that adhere to its surface, do not impose mechanical impedance (e.g., exhibit low modulus) upon actuation, and maintain their electrical properties during elongation and contraction of the dielectric film (artificial muscle). Conventionally, electrodes made, e.g., from carbon grease or graphite spray are employed because they provide sufficient electrical conductivity and have negligible modulus [33].

Based on the concept of dielectric actuators, tunable optical devices such as retarder plates

[35], optical gratings with an adjustable pitch [36,37] or phase contrast [38], as well as photonic bandgap composites with rejection wavelength tuning [39] have been developed. In all of these devices, the optically active component is either the artificial muscle itself [35,39] or (in the case of devices used in reflection) a separate active layer on top of one of the compliant electrodes [36,37]. While the employed grease electrodes have been proven useful, they have the severe disadvantages of being optically opaque and having a nonpatternable surface, which prevents them from being the optically active part of the device. In practical devices, their exposure to the environment needs to be avoided as they are not resistant to mechanical damage, which requires a more sophisticated electrode design and complicates system assembly [25,36].

Here, we demonstrate a design for tunable optical devices based on the artificial muscle concept in which the compliant electrodes are bifunctional and serve both as electronic conductors and optically active layer. This is achieved by employing elastomeric compliant electrode thin films consisting of a  $\approx 30 \mu\text{m}$  thick layer of electrically conductive and patternable silicone elastomer [poly(dimethyl siloxane) (PDMS)] composite. In two proof-of-concept demonstrations of our approach, we show the actuation of an imprinted diffraction grating and of polymer-infiltrated colloidal crystals with photonic properties.

While using an actuated elastomeric layer as a diffraction grating or structural color element, similar to previous work in the field [37,39], our work combines the enhanced electromechanical properties of a polymer nanocomposite with optical functionality and, thus, represents a compact and simple approach for electrostatically actuated optical elements.

## 2. Compliant Electrode and Actuator Fabrication

### A. Fabrication and Characterization of the Conducting Nanocomposite

In order to render PDMS electrically conductive for use as a compliant electrode, we chose functionalized graphene sheets (FGSs) [40–43] as the filler material. FGSs exhibit a large specific surface area in the range of 600 to 1850  $\text{m}^2/\text{g}$  (measured by nitrogen adsorption on the dry powder (BET) and by Methylene Blue dye adsorption in a suspension form) [40,41], high aspect ratio (atomically thin sheets with diameters on the order of  $1 \mu\text{m}$  [40,41]), and, consequently, a low electrical percolation threshold [43] as well as good dispersability in solvents in which silicone elastomer precursors can be dissolved.

We prepared our electrodes according to the following recipe: FGSs were suspended in tetrahydrofuran (THF) at a concentration of 0.6 mg/ml by tip-ultrasonication for 30 min. A PDMS precursor (Wacker RT625) was diluted with THF at a volume ratio of 1:1 and mixed with the filler suspension. An appropriate amount of cross-linker and catalyst was added (the adsorption of cross-linker and catalyst

on the FGSs had to be taken into account [43]), and the resulting slurry was cast in a thin film on the bottom of a plastic Petri dish. Subsequently, curing was done for 24 h at 70 °C. The electrode thickness was determined by imaging of a cross section with a scanning electron microscope (SEM).

The electrical conductivity of composite films was measured by recording current-voltage curves of  $1 \text{ cm} \times 3 \text{ cm}$  electrode strips in a classical four-point-probe configuration using a computer-controlled potentiostat (SP-150, BioLogic USA, LLC). Mechanical testing of the electrode films and the artificial muscle was performed using an Instron 5567A mechanical tester with a 50 N load cell. Values for the modulus were reported in terms of engineering stress. For measurements of the electrical conductivity as a function of electrode strain, two electrical contacts were attached to the (electrically insulated) clamps of the mechanical tester, and the resistance of the sample held by the clamps was continuously monitored with an electrometer (Keithley 6517A).

### B. Preparation of Optical Components

For our first demonstration with patterned silicone rubber electrodes, we pressed a diffraction grating master (holographic diffraction grating film, 1000 lines/mm, Rainbow Symphony, Reseda, Calif.) into the composite film before curing. After curing, the grating master was peeled off, and the patterned PDMS electrodes were cut into the desired shape and peeled off the Petri dish. Figure 1(a) shows an SEM image of an electrode film with imprinted diffraction grating using 1.5 wt.% FGS in PDMS. The periodic structure of the diffraction grating on the front surface is evident.

For our second demonstration, with infiltrated colloidal crystals, we prepared our samples according to the following protocol: a silicon wafer was cleaned by etching in 1 M potassium hydroxide solution and then mildly oxidized for 1 min in piranha solution to render it hydrophilic. The wafer was placed in a Petri dish, and a stock suspension of polystyrene (PS) particles (8 g/100 ml, as purchased, Invitrogen Corp., Carlsbad, Calif.) was dripped onto the surface (about 10 drops for one 3 in. wafer) and distributed by careful swirling of the Petri dish. The coated wafer was allowed to dry overnight in air at room temperature. With this simple approach, we obtained face-centered-cubic (fcc) colloidal crystals [Fig. 1(b)] with a typical thickness of about  $5 \mu\text{m}$  and single crystalline domains extending laterally over more than  $100 \mu\text{m}$  (as determined from SEM images) that showed bright structural color [see the inset of Fig. 1(b)]. In the next step, we fabricated the patterned compliant electrode by spin coating the FGS/PDMS slurry onto the colloidal crystal created by evaporative drying. The spin-coated layer was then cured and subsequently peeled off the silicon wafer. Because the PDMS matrix infiltrates the interstitials of the colloidal crystal, PS spheres are embedded in the polymer matrix [Fig. 1(c)].

Although we tried to decrease the thickness of the electrode films as far as possible to increase electrode compliance, our attempts were limited by practical considerations because after curing, the composite films needed to be peeled off the curing substrate. Thus, the electrode thickness both for the diffraction grating samples as well as the films bearing embedded colloidal crystals was typically between 30 and 50  $\mu\text{m}$ .

We prepared infiltrated colloidal crystals with different lattice dimensions employing PS spheres with diameters of 300 and 600 nm. Because of the small size of the interstitials ( $<75$  nm) [44] of the fcc crystal compared to the size of the FGSs (single sheets typically exhibit diameters between 0.1 and 1  $\mu\text{m}$  [40,41]), graphene sheets do not enter the interstitial volume of the colloidal crystal. Therefore, the fraction of the polymer that infiltrates the colloid layer is not electrically conductive, and by attempting to infiltrate the colloidal crystals with the slurry we conveniently create an inherently bonded two-layer structure due to the filtering effect of the colloidal crystal. The colloidal crystal now serves as the dielectric component of our system, while the part of the composite film that did not infiltrate the colloid layer is filled with graphene and, therefore, exhibits electrical conductivity. This filtering effect avoids optical absorption due to FGSs in the colloidal layer completely if the layer of infiltrated colloidal particles is sufficiently thick to allow light waves with the rejection wave length to decay within the dielectric part of the bilayer.

### C. Actuator Assembly

Using these patterned FGS/PDMS electrodes, we assembled our tunable optical elements in the following way [Fig. 1(d)]. We used prestretched acrylic film (VHB 4910, 3M, Livonia, Michigan) as the dielectric actuator due to its large actuation amplitudes [31]. The acrylic film was fixed on a rigid metal ring with a diameter of 8 cm under a biaxial prestrain of 200% (corresponding to a nine-fold surface area increase). On top, a patterned and cured rectangular silicone rubber electrode ( $\approx 1$   $\text{cm}^2$ ) was directly attached to the center of the film. The optically “active” layer, i.e., the imprinted diffraction grating or the infiltrated colloidal crystal, is faceup on the acrylic film.

Also, the electrical connection to the electrode was made from our conductive silicone elastomer. The bottom electrode was fabricated by smearing carbon grease of a similar shape directly onto the acrylic film in order to reduce mechanical impedance and maximize the actuation amplitude. Our devices were actuated by applying voltage pulses of up to 6 kV at a frequency of 0.5 Hz or linear voltage ramps using a function generator (PFG5105 from Tektronix, Inc., Beaverton, Oreg.) and a high-voltage amplifier (TREK Model 20/20C, TREK Inc., Medina, N.Y.).

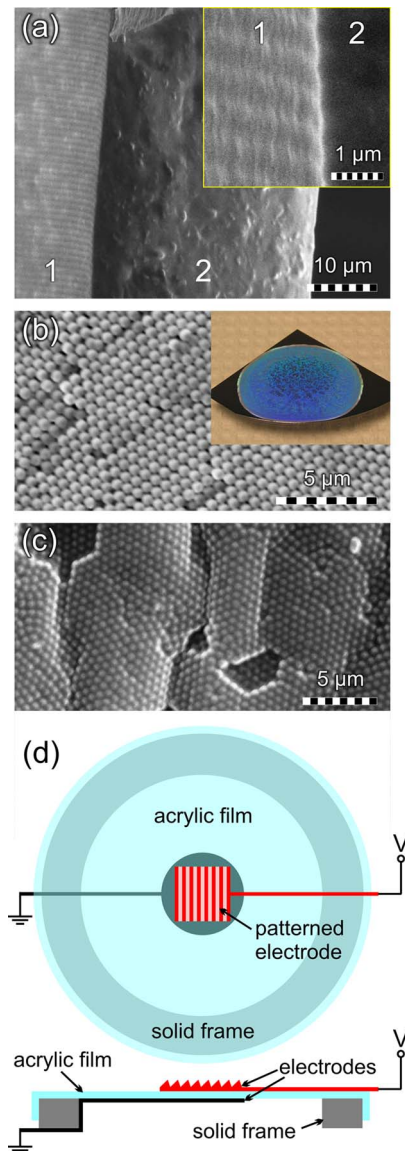


Fig. 1. (Color online) (a) SEM images of an FGS-filled silicone rubber electrode with imprinted diffraction grating. The imprinted grating on the top surface can be seen on the left of the image (1), while the center shows the cross-sectional area of the electrode (2). (b) SEM image of a colloidal crystal consisting of 600 nm PS microspheres. Inset, photo of colloidal crystal on a quarter of a 3 in. silicon wafer before infiltration. (c) SEM image of 600 nm PS spheres embedded in the PDMS electrode. (d) Sketch of the experimental setup used for actuation, top and side view.

### 3. Electrical and Mechanical Properties of Compliant Electrodes

Here, we characterize the basic electrical and mechanical properties of our composites and then, in the following sections, demonstrate the actuation of electrodes with imprinted diffraction grating as well as with a photonic structure exhibiting an infrared (IR) stop band.

The performance of the electrostatic actuators depends largely on the proper design of the compliant electrodes [33]. For example, the actuation speed is not only limited by viscoelastic losses and the speed

of sound in the actuator material, but also by the time needed to charge the electrodes (electrical response time). The latter can be estimated by calculating the time constant  $\tau = R \cdot C$  of the actuator, where resistance,  $R$ , and capacitance,  $C$ , are defined by the actuator geometry. It follows, that for a device with  $10 \text{ mm}^2$  area,  $60 \text{ }\mu\text{m}$  thick acrylic film of relative permittivity,  $\epsilon_r = 3$ , electrode thickness of  $20 \text{ }\mu\text{m}$ , and a desired electrical response time of  $1 \text{ ms}$ , a conductivity of about  $0.01 \text{ S/m}$  is sufficient. Using acrylic film as an artificial muscle, the actual actuator response time in our system is limited by the mechanical properties of the actuator film, which results in a time constant on the order of seconds [32]. However, electrodes with a fast electrical response time will also be applicable in devices operating with artificial muscles that have a faster mechanical response.

In order to achieve sufficient conductivity for our application, we tested FGS/PDMS compliant electrodes with varying FGS loadings. At a concentration of  $1.5 \text{ wt.}\%$ , the FGSs appear to have formed agglomerates within the polymer matrix [Fig. 1(a)]. This might be due to difficulties during the mixing of the slurry, because with FGSs the viscosity is drastically increased. We therefore reduced the filler concentration subsequently and found that even at  $0.8 \text{ wt.}\%$  filler loading, the resulting films show large conductivity ( $\approx 1.5 \text{ S/m}$ ), by far exceeding the limit estimated from the RC time scale of the actuator ( $0.01 \text{ S/m}$ ), while the FGS slurry exhibits a significantly smaller viscosity, which improves electrode processing and filler dispersion.

Because a compliant electrode needs to retain its conductivity upon the application of strain, we measured the conductivity of our FGS-filled electrodes as a function of elongation by attaching the two ends of an electrode strip (dimensions  $22.55 \text{ mm} \times 4.55 \text{ mm} \times 300 \text{ }\mu\text{m}$ ) to a mechanical tester (Instron 5567A). Electrodes with FGS loadings equal or greater than  $0.8 \text{ wt.}\%$  typically remain sufficiently electrically conducting ( $>0.01 \text{ S/m}$ , see above) up to a mechanical strain that exceeds the values necessary for full color tuning ( $\approx 25\%$ , see Appendix A).

The moduli of FGS/PDMS composites increase with FGS content (up to  $3 \text{ MPa}$  at  $1 \text{ wt.}\%$  loading with FGSs, depending on the degree of cross-linking). A modulus of the  $60 \text{ }\mu\text{m}$  thick prestrained acrylic film (artificial muscle) is more difficult to obtain. While in the absence of prestrain, we measure a Young modulus of about  $0.25 \text{ MPa}$  under uniaxial stretching, the modulus at break ( $\sim 1000\%$  uniaxial strain) is about  $0.75 \text{ MPa}$ . In an actuator configuration, the acrylic film is biaxially prestrained. However, the electrodes only occupy a small fraction of the total surface area of the artificial muscle. Therefore, while the area between the electrodes is undergoing lateral extension, the surrounding acrylic film is relaxed. This significantly reduces the force necessary to induce mechanical deformation through Maxwell stress.

Because a detailed analysis of the mechanical properties of the artificial muscle is beyond the scope

of this paper, we can only contend that the  $\approx 30 \text{ }\mu\text{m}$  thick compliant electrode is responsible for a significant fraction of the tensile stress opposing actuation, and we did not try to minimize the modulus of the electrode because our main goal in this study was to provide a proof-of-concept demonstration.

#### 4. Tunable Diffraction Grating

A schematic of the optical setup used for the measurement of changes in the pitch of the diffraction grating imprinted on our compliant electrode is shown in Fig. 2(a). The electrode is illuminated with collimated white light from a halogen lamp. A CCD camera is positioned about  $20 \text{ cm}$  away from the diffraction grating at the location of the first-order diffraction spectrum. The distance is chosen such that the imaging aperture is sufficiently small to allow for the observation of a distinct color under the given diffraction angle (high-aperture imaging would lead to color averaging).

Upon application of voltage pulses, a color change from blue to green is observed [Fig. 2(b)]. However, the lateral expansion of the acrylic film and the top electrode is not evident in the images. Therefore, we changed the position of the camera and switched to diffuse light illumination, so that the circumference of the silicone rubber electrode becomes visible

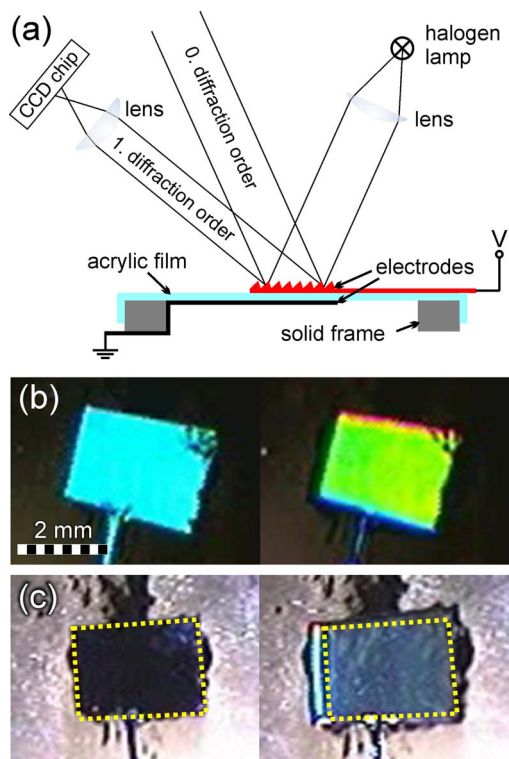


Fig. 2. (Color online) (a) Schematic of optical setup for tests with tunable diffraction gratings. (b) Color change of an actuated grating at an applied voltage of  $6 \text{ kV}$  and a frequency of  $0.5 \text{ Hz}$ . Left, relaxed state; right, maximum actuation at  $6 \text{ kV}$ . The patterned electrode is filled with  $1 \text{ wt.}\%$  FGS. (c) Same grating as in (b) shown under diffuse illumination to illustrate lateral expansion. The dotted yellow line indicates the boundaries of the nonactuated electrode.

on a bright background of light directly reflected from the uncoated acrylic film [Fig. 2(c)]. From the blue and green colors in Fig. 2(b), we estimate an increase in the wavelength of the observed reflected light from approximately 470 to 530 nm. The wavelength  $\lambda$  of diffracted light at a given diffraction angle  $\alpha$  in the first diffraction order is proportional to the lattice period  $d$  of the grating:  $\lambda = d \sin(\alpha)$ . The observed increase of the wavelength (13%) is in agreement with the observed lateral expansion of the electrode by about 14% [Fig. 2(c)], causing a corresponding increase of  $d$ . An actuation amplitude of 25%, necessary for covering a large fraction of the color space (see Appendix A), can be achieved by further optimization of our setup, such as using thinner acrylic film and thinner compliant electrodes.

Because the FGSs exhibit optical absorption (FGS powder appears black), the question arises to what extent this absorption may improve the optical performance (reflectivity) of the grating. However, our black FGS/PDMS composites only show the weak reflectivity typical for the reflections from the surface of the neat polymer. We estimate that the optical absorption length of our composite is at least on the order of  $4 \mu\text{m}$  (see Appendix B). Consequently, compared to a metallic surface, the attenuation is small and has only a negligible effect on the sample reflectivity. It follows that additional reflective coatings need to be applied in order to achieve a reflectivity suitable for applications. The feasibility of this has been shown for dynamically actuated polymeric optical components [36].

### 5. Tunable Photonic Structure

While, due to the observation-angle dependence of the color of the diffracted light, the application of actuated diffraction gratings is limited to filtering purposes, e.g., in wavelength-adjustable luminous sources, it is necessary to switch to more complex photonic structures for the creation of optical devices that can be directly used as pixels in an optical display application, particularly under daylight illumination. We analyze the applicability of our material for tunable structural color pixel displays based on photonic materials coupled with our compliant electrode below.

In our first attempt, we actuated a PDMS-infiltrated colloidal crystal made from 600 nm PS spheres. This structure exhibits an insufficient refractive index contrast between the silicone elastomer and the PS spheres ( $n_{\text{PDMS}} = 1.39$ ,  $n_{\text{PS}} = 1.59$ , both taken from the literature [45]) and a too large lattice constant to show a photonic band gap, and therefore optically behaves like a two-dimensional diffraction grating. But it can, in a first step, be used to prove that a lateral stretching of the optically active layer occurs during actuation of the underlying artificial muscle. Upon electrical actuation of the assembled device, the observed color in the first diffraction order changes from green to red [Figs. 3(a) and 3(b)]. This indicates that an increase of the lateral distance between the particles within the PDMS-infiltrated col-

loidal crystal occurs, giving an effect similar to our observations with the diffraction grating [Fig. 2(b)]: an increase in lateral interparticle spacing leads to an increase in the wavelength of the diffracted light at a given diffraction angle. This observation cannot be related to the Bragg reflection between different lateral planes (normal to the incident light beam) of the infiltrated colloidal crystal because a medial compression of the film, which decreases the  $d$  spacing between lateral crystal planes, would decrease the wavelength [25], which is not observed.

In order to achieve true photonic crystal properties, we infiltrated a colloidal crystal produced with smaller (300 nm) PS spheres. We measured the reflection spectrum with a glass fiber probe attached to a spectrometer (Filmetrics) [Fig. 3(c)] and observed a sharp IR reflection peak measured under normal incidence at a numerical aperture of about

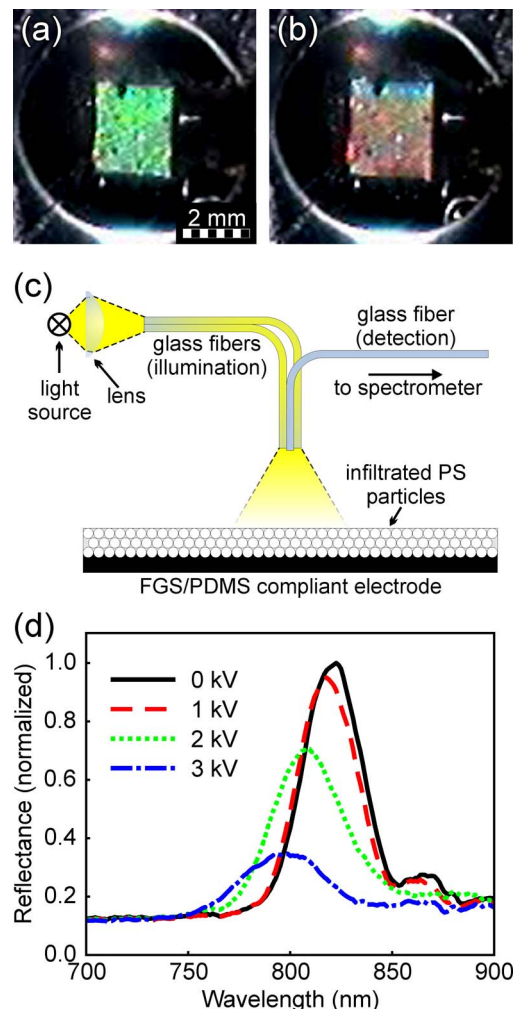


Fig. 3. (Color online) (a), (b) Color change of an electrode with an infiltrated layer of 600 nm PS spheres. The relaxed state (a) and actuated state (b) at an applied voltage of 6 kV are shown. Because of inhomogeneities of the infiltrated colloidal crystal, the color of the structure is nonhomogeneous. (c) Schematic of setup used for spectroscopic analysis of light reflected from compliant electrodes with photonic properties. (d) IR stop band shift of an electrode with infiltrated 300 nm PS spheres.

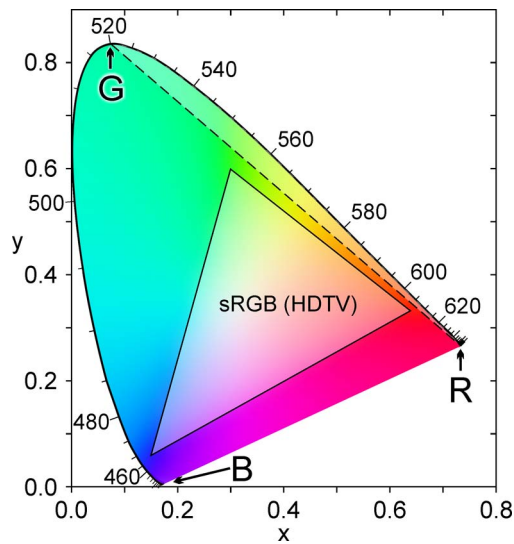


Fig. 4. (Color online) Map of colors perceivable to the human eye (CIE 1931). By additive mixing of the spectral color red (R,  $\sim 640$  nm) with tunable structural color in the range from spectral blue (B,  $\sim 440$  nm) to green (G,  $\sim 520$  nm), almost the entire color space can be covered. The triangle in the center indicates the sRGB color space, which can be generated by modern computer displays and television units.

0.2 (based on the acceptance cone of the optical fiber). During actuation, we were able to shift this peak from 825 nm in the nonactuated state to 795 nm upon application of 3 kV [Fig. 3(d)]. The decrease in wavelength indicates that the Bragg reflection at the compressed PS layers causes the observed IR peak and that we created a material with an optical stop band. We also observed a decrease in reflectance during actuation, accompanied by a slight ( $\sim 10\%$ ) increase of the full width at half-maximum of the peak, which indicates a degradation of the photonic properties of the material. This may likely be related to the fact that upon lateral stretching of the photonic film, the lateral spacing between the embedded PS spheres becomes larger, allowing them to become more interdigitated as the  $d$  spacing decreases. This decreases the dielectric contrast between the Bragg layers, which causes the decrease in reflectivity.

If colloidal crystals with even smaller particles ( $< 300$  nm in diameter) were used, a similar observation of a tunable stop band in the visible range can be expected. However, such silicone infiltrated colloidal crystals are more difficult to obtain because the infiltration technique is length-scale dependent. As the particle size decreases, the volume-specific surface area of the colloidal crystal increases, thus impeding the capillary infiltration of the polymer precursor due to increased porous medium resistance. A potential solution for this issue involves the adaptation of a PDMS precursor with lower viscosity, such that the infiltration would occur at a higher rate.

## 6. Conclusions

We have developed a technique to build dynamically tunable optical devices by employing the compliant electrodes of dielectric actuators as optically active

layers. We use silicone rubber filled with graphene, which exhibits a conductivity of  $\approx 1.5$  S/m at filler concentrations of 0.8 wt.%. Upon strain, the material retains a conductivity  $> 0.01$  S/m which we estimated to be sufficient for an electrical response time of 1 ms. The electrodes can be given arbitrary shapes, and they adhere readily on the acrylic film used as artificial muscle. We demonstrated the use of our electrode design for the dynamic tuning of structural color employing imprinted diffraction gratings and infiltrated colloidal crystals.

This work was supported by United States Army Research Office (USARO)/Multidisciplinary University Research Initiative through grants W911NF-04-1-0170 and W911F-09-1-0476 and by the National Aeronautics and Space Administration (NASA) University Research, Engineering, and Technology Institute on BioInspired Materials under award NCC-1-02037. C.Punckt acknowledges financial support from the Alexander von Humboldt Foundation. Discussions with Shuyang Pan were greatly appreciated.

## Appendix A: Tunable Structural Color for Display Applications

The use of structural color for display devices has the potential of accessing the full range of colors perceivable to the human eye. This is illustrated in Fig. 4, where we show an image of the CIE 1931 color space. While, e.g., liquid crystal displays, which are based on the red-green-blue (RGB) color scheme, can only produce colors within a given triangle that lies inside the color space (see shaded triangle in Fig. 4), structural color devices can, in theory, cover the full color space.

This can be achieved by additive mixing of two colors on the spectral locus (the horseshoe-shaped boundary of the color space) using, e.g., red as the fixed color (point R in Fig. 4) and varying the other color dynamically along the spectral colors. Interestingly, almost the whole color space can be reproduced by varying the dynamic color between blue (B) and green (G). Then, only the small shaded area at the top right of the color space (separated by a dashed line in Fig. 4) is inaccessible. The wavelengths corresponding to points B and G are about 440 and 520 nm, respectively, which is an increase of less than 20%. Because the wavelength  $\lambda$  equals the product of the sine of the (fixed) diffraction angle and the lattice period  $d$ , tuning of the dynamic color in this range can be achieved by varying the pitch of an elastic diffraction grating used as color filter by 20%. Additive mixing with the (fixed) spectral color red (R) can then produce almost any perceivable color by dynamically varying the pitch of the grating. As electrostatic actuators have been shown to exceed elongations of 100% [31] and to respond on acoustic time scales [34], such devices are, in general, suitable for structural color tuning.

## Appendix B: Estimation of Composite Reflectivity

Our estimate is based on the fact that a single layer of perfect graphene has an optical absorption of

$\pi \cdot \alpha \approx 2.3\%$ , where  $\alpha$  is the fine structure constant (normal incidence) [46]. Correspondingly, it will take  $-1/\ln(1 - \pi \cdot \alpha) \approx 43$  layers of graphene to absorb  $(1 - 1/e) \approx 63\%$  of the incoming light. Using the specific gravities of PDMS ( $0.97 \text{ g/cm}^3$ ) and graphite ( $2.2 \text{ g/cm}^3$ ), we calculated that the light will have to go through approximately  $4 \mu\text{m}$  of composite in order to pass 43 layers of graphene at our filler loading of 0.8 wt.%. If the optical properties of our FGS/PDMS composite are expressed by an effective complex index of refraction  $\hat{n} = n(1 + i\kappa)$ , an absorption length of  $4 \mu\text{m}$  corresponds to an attenuation coefficient  $\kappa \approx 0.0084$  (at wavelength  $\lambda = 589.3 \text{ nm}$ ). Therefore, the reflectivity is essentially determined by the real part of the refractive index, which, at the given low filler loading, is most likely close to the value of bulk PDMS ( $n = 1.39$ ).

Additionally, our approach overestimates the absorption because FGSs have a lower conductivity than perfect graphene and because the sheets in the composite are randomly oriented while the estimate assumes normal illumination. There will also be a small correction of the weight per layer of graphene due to the functional groups at the FGS surface. Hence, a more rigorous analysis of the optical properties of FGS-polymer nanocomposites will be necessary in the future.

## References and Notes

- H. Ghiradella, "Light and color on the wing—structural colors in butterflies and moths," *Appl. Opt.* **30**, 3492–3500 (1991).
- A. R. Parker, "515 million years of structural colour," *J. Opt. A Pure Appl. Opt.* **2**, R15–R28 (2000).
- P. Vukusic and J. R. Sambles, "Photonic structures in biology," *Nature* **424**, 852–855 (2003).
- S. Yoshioka and S. Kinoshita, "Single-scale spectroscopy of structurally colored butterflies: measurements of quantified reflectance and transmittance," *J. Opt. Soc. Am. A* **23**, 134–141 (2006).
- R. T. Lee and G. S. Smith, "Detailed electromagnetic simulation for the structural color of butterfly wings," *Appl. Opt.* **48**, 4177–4190 (2009).
- J. M. Weissman, H. B. Sunkara, A. S. Tse, and S. A. Asher, "Thermally switchable periodicities and diffraction from mesoscopically ordered materials," *Science* **274**, 959–960 (1996).
- H. Fudouzi and Y. N. Xia, "Colloidal crystals with tunable colors and their use as photonic papers," *Langmuir* **19**, 9653–9660 (2003).
- P. Jiang, D. W. Smith, J. M. Ballato, and S. H. Foulger, "Multi-color pattern generation in photonic bandgap composites," *Adv. Mater.* **17**, 179–184 (2005).
- C. Paquet and E. Kumacheva, "Nanostructured polymers for photonics," *Mater. Today* **11**, 48–56 (2008).
- J. H. Holtz and S. A. Asher, "Polymerized colloidal crystal hydrogel films as intelligent chemical sensing materials," *Nature* **389**, 829–832 (1997).
- D. Nakayama, Y. Takeoka, M. Watanabe, and K. Kataoka, "Simple and precise preparation of a porous gel for a colorimetric glucose sensor by a templating technique," *Angew. Chem.* **42**, 4197–4200 (2003).
- H. Fudouzi and T. Sawada, "Photonic rubber sheets with tunable color by elastic deformation," *Langmuir* **22**, 1365–1368 (2006).
- Y. Kang, J. J. Walish, T. Gorishnyy, and E. L. Thomas, "Broad-wavelength-range chemically tunable block-copolymer photonic gels," *Nat. Mater.* **6**, 957–960 (2007).
- M. Harun-Ur-Rashid, T. Seki, and Y. Takeoka, "Structural colored gels for tunable soft photonic crystals," *Chem. Rec.* **9**, 87–105 (2009).
- J. R. Lawrence, Y. R. Ying, P. Jiang, and S. H. Foulger, "Dynamic tuning of organic lasers with colloidal crystals," *Adv. Mater.* **18**, 300–303 (2006).
- O. Solgaard, F. S. A. Sandejas, and D. M. Bloom, "Deformable grating optical modulator," *Opt. Lett.* **17**, 688–690 (1992).
- K. Sumioka, H. Kayashima, and T. Tsutsui, "Tuning the optical properties of inverse opal photonic crystals by deformation," *Adv. Mater.* **14**, 1284–1286 (2002).
- L. Xu, J. X. Wang, Y. L. Song, and L. Jiang, "Electrically tunable polypyrrole inverse opals with switchable stopband, conductivity, and wettability," *Chem. Mater.* **20**, 3554–3556 (2008).
- Y. J. Lu, H. W. Xia, G. Z. Zhang, and C. Wu, "Electrically tunable block copolymer photonic crystals with a full color display," *J. Mater. Chem.* **19**, 5952–5955 (2009).
- J. J. Walish, Y. Kang, R. A. Mickiewicz, and E. L. Thomas, "Bioinspired electrochemically tunable block copolymer full color pixels," *Adv. Mater.* **21**, 3078–3081 (2009).
- K. Ueno, J. Sakamoto, Y. Takeoka, and M. Watanabe, "Electrochromism based on structural colour changes in a polyelectrolyte gel," *J. Mater. Chem.* **19**, 4778–4783 (2009).
- A. C. Arsenault, D. P. Puzzo, I. Manners, and G. A. Ozin, "Photonic-crystal full-colour displays," *Nat. Photon.* **1**, 468–472 (2007).
- D. P. Puzzo, A. C. Arsenault, I. Manners, and G. A. Ozin, "Electroactive inverse opal: a single material for all colors," *Angew. Chem.* **48**, 943–947 (2009).
- Z. F. Liu, T. Ding, G. Zhang, K. Song, K. Clays, and C. H. Tung, "Ternary inverse opal system for convenient and reversible photonic bandgap tuning," *Langmuir* **24**, 10519–10523 (2008).
- S. H. Foulger, P. Jiang, A. Lattam, D. W. Smith, J. Ballato, D. E. Dausch, S. Grego, and B. R. Stoner, "Photonic crystal composites with reversible high-frequency stop band shifts," *Adv. Mater.* **15**, 685–689 (2003).
- M. Honda, T. Seki, and Y. Takeoka, "Dual tuning of the photonic band-gap structure in soft photonic crystals," *Adv. Mater.* **21**, 1801–1804 (2009).
- Y. S. Yang, Y. H. Lin, Y. C. Hu, and C. H. Liu, "A large-displacement thermal actuator designed for MEMS pitch-tunable grating," *J. Micromech. Microeng.* **19**, 015001 (2009).
- C. W. Wong, Y. Jeon, G. Barbastathis, and S. G. Kim, "Analog tunable gratings driven by thin-film piezoelectric microelectromechanical actuators," *Appl. Opt.* **42**, 621–626 (2003).
- X. Li, C. Antoine, D. S. Lee, J. S. Wang, and O. Solgaard, "Tunable blazed gratings," *J. Microelectromech. Syst.* **15**, 597–604 (2006).
- Y. J. Wang, Y. Kanamori, and K. Hane, "Pitch-variable blazed grating consisting of freestanding silicon beams," *Opt. Express* **17**, 4419–4426 (2009).
- R. Pelrine, R. Kornbluh, Q. B. Pei, and J. Joseph, "High-speed electrically actuated elastomers with strain greater than 100%," *Science* **287**, 836–839 (2000).
- F. Carpi, P. Chiarelli, A. Mazzoldi, and D. De Rossi, "Electromechanical characterisation of dielectric elastomer planar actuators: comparative evaluation of different electrode materials and different counterloads," *Sens. Actuators A Phys.* **107**, 85–95 (2003).
- A. O'Halloran, F. O'Malley, and P. McHugh, "A review on dielectric elastomer actuators, technology, applications, and challenges," *J. Appl. Phys.* **104**, 071101 (2008).

34. R. Heydt, R. Pelrine, J. Joseph, J. Eckerle, and R. Kornbluh, "Acoustical performance of an electrostrictive polymer film loudspeaker," *J. Acoust. Soc. Am.* **107**, 833–839 (2000).
35. M. Beck, R. Fiolka, and A. Stemmer, "Variable phase retarder made of a dielectric elastomer actuator," *Opt. Lett.* **34**, 803–805 (2009).
36. M. Aschwanden and A. Stemmer, "Polymeric, electrically tunable diffraction grating based on artificial muscles," *Opt. Lett.* **31**, 2610–2612 (2006).
37. M. Aschwanden, M. Beck, and A. Stemmer, "Diffractive transmission grating tuned by dielectric elastomer actuator," *IEEE Photon. Technol. Lett.* **19**, 1090–1092 (2007).
38. S. Uma, R. Matusiak, D. L. Hecht, and E. J. Shrader, "Elastomer-based diffractive optical modulator," *IEEE J. Sel. Top. Quant. Electron.* **10**, 435–439 (2004).
39. J. Q. Xia, Y. R. Ying, and S. H. Foulger, "Electric-field-induced rejection wavelength tuning of photonic bandgap composites," *Adv. Mater.* **17**, 2463–2467 (2005).
40. H. C. Schniepp, J. L. Li, M. J. McAllister, H. Sai, M. Herrera-Alonso, D. H. Adamson, R. K. Prud'homme, R. Car, D. A. Saville, and I. A. Aksay, "Functionalized single graphene sheets derived from splitting graphite oxide," *J. Phys. Chem. B* **110**, 8535–8539 (2006).
41. M. J. McAllister, J. L. Li, D. H. Adamson, H. C. Schniepp, A. A. Abdala, J. Liu, M. Herrera-Alonso, D. L. Milius, R. Car, R. K. Prud'homme, and I. A. Aksay, "Single sheet functionalized graphene by oxidation and thermal expansion of graphite," *Chem. Mater.* **19**, 4396–4404 (2007).
42. T. Ramanathan, A. A. Abdala, S. Stankovich, D. A. Dikin, M. Herrera-Alonso, R. D. Piner, D. H. Adamson, H. C. Schniepp, X. Chen, R. S. Ruoff, S. T. Nguyen, I. A. Aksay, R. K. Prud'homme, and L. C. Brinson, "Functionalized graphene sheets for polymer nanocomposites," *Nat. Nanotechnol.* **3**, 327–331 (2008).
43. S. Pan, S. Sanborn, S. Korkut, L. J. Gibbons, E. J. Siochi, J.-H. Prévost, R. K. Prud'homme, and I. A. Aksay are preparing a manuscript to be called "Distributed deformation in multi-functional graphene-silicone elastomer nanocomposite."
44. The interstitial size is  $\approx 1/8$  of the PS sphere size.
45. A. C. M. Kuo and Z. Pu, *Polymer Data Handbook*, 2nd ed. (Oxford University Press, 2009).
46. P. E. Gaskell, H. S. Skulason, C. Rodenchuk, and T. Szkopek, "Counting graphene layers on glass via optical reflection microscopy," *Appl. Phys. Lett.* **94**, 143101 (2009).